AMERICAN SOCIETY FOR MICROBIOLOGY | Journal of Virology®

PATHOGENESIS AND IMMUNITY

Coronavirus Endoribonuclease and Deubiquitinating Interferon Antagonists Differentially Modulate the Host Response during Replication in Macrophages

Aaron Volk,[a] Matthew Hackbart,[a] Xufang Deng,[a] Yazmin Cruz-Pulido,[a] Amornrat O'Brien,[a] Susan C. Baker[a]

[a]Department of Microbiology and Immunology, Loyola University Chicago Stritch School of Medicine, Maywood, Illinois, USA

Aaron Volk and Matthew Hackbart contributed equally to this work.

ABSTRACT Coronaviruses (CoVs) encode multiple interferon (IFN) antagonists that modulate the host response to virus replication. Here, we evaluated the host transcriptional response to infection with murine coronaviruses encoding independent mutations in one of two different viral antagonists, the deubiquitinase (DUB) within nonstructural protein 3 or the endoribonuclease (EndoU) within nonstructural protein 15. We used transcriptomics approaches to compare the scope and kinetics of the host response to the wild-type (WT), DUBmut, and EndoUmut viruses in infected macrophages. We found that the EndoUmut virus activates a focused response that predominantly involves type I interferons and interferon-related genes, whereas the WT and DUBmut viruses more broadly stimulate upregulation of over 2,800 genes, including networks associated with activating the unfolded protein response (UPR) and the proinflammatory response associated with viral pathogenesis. This study highlights the role of viral interferon antagonists in shaping the kinetics and magnitude of the host response during virus infection and demonstrates that inactivating a dominant viral antagonist, the coronavirus endoribonuclease, dramatically alters the host response in macrophages.

IMPORTANCE Macrophages are an important cell type during coronavirus infections because they "notice" the infection and respond by inducing type I interferons, which limits virus replication. In turn, coronaviruses encode proteins that mitigate the cell's ability to signal an interferon response. Here, we evaluated the host macrophage response to two independent mutant coronaviruses, one with reduced deubiquitinating activity (DUBmut) and the other containing an inactivated endoribonuclease (EndoUmut). We observed a rapid, robust, and focused response to the EndoUmut virus, which was characterized by enhanced expression of interferon and interferon-related genes. In contrast, wild-type virus and the DUBmut virus elicited a more limited interferon response and ultimately activated over 2,800 genes, including players in the unfolded protein response and proinflammatory pathways associated with progression of significant disease. This study reveals that EndoU activity substantially contributes to the ability of coronaviruses to evade the host innate response and to replicate in macrophages.

KEYWORDS IFN antagonist, PLP2, coronavirus, EndoU, nsp15, papain-like protease, transcriptomic profiling

The ability to evade or delay activation of host innate and adaptive immune responses is now recognized as an important characteristic of many pathogenic viruses. Viruses from diverse families, including filoviruses (1), poxviruses (2), influenza viruses (3), flaviviruses (4), and coronaviruses (CoVs) (5, 6), encode proteins that are not required for viral replication *per se* but which act as modulators of initial, innate host

Citation Volk A, Hackbart M, Deng X, Cruz-Pulido Y, O'Brien A, Baker SC. 2020. Coronavirus endoribonuclease and deubiquitinating interferon antagonists differentially modulate the host response during replication in macrophages. J Virol 94:e00178-20. https://doi.org/10.1128/JVI.00178-20.

Editor Bryan R. G. Williams, Hudson Institute of Medical Research

Address correspondence to Susan C. Baker, sbaker1@luc.edu.

For a companion article on this topic, see https://doi.org/10.1128/JVI.01734-19.

Received 6 February 2020
Accepted 9 March 2020
Accepted manuscript posted online 18 March 2020
Published 18 May 2020

responses or of later, adaptive responses that aim to limit virus replication. By understanding how these viral antagonists regulate the immune response, we can fine-tune the rational design of therapeutics and vaccines to control existing and emerging viral pathogens.

Coronaviruses (CoVs) are characterized in part by their large (~30 kb), positive-sense single-stranded RNA genomes that yield a nested set of subgenomic mRNAs during viral replication (6, 7). These large genomes encode the replicase polyprotein, the canonical structural proteins (spike, envelope, membrane, and nucleocapsid), and, depending on the CoV, a number of accessory genes. Notably, many of these different genes (replicase, structural, and accessory) encode proteins that regulate the antiviral response, indicating that viral antagonists of host defenses play an important role during infection (8–12). In this report, we investigate the role(s) of two highly conserved enzymatic domains within the replicase polyprotein of mouse hepatitis virus (MHV)—the viral protease/deubiquitinase (DUB) and the endoribonuclease (EndoU)—in altering host immune responses.

The replicase polyprotein machinery must be processed into its functional parts during viral replication, which, in the case of MHV, requires the activity of three proteases, two papain-like proteases (PLP1 and PLP2) and one chymotrypsin-like protease (3CLpro, sometimes referred to as Mpro). MHV PLP2 is structurally similar to the single papain-like protease (termed PLpro) encoded by severe acute respiratory syndrome coronavirus (SARS-CoV) and Middle East respiratory syndrome coronavirus (MERS-CoV). Previous studies demonstrated that CoV PLP2s/PLpros are multifunctional, with catalytic residues that mediate protease, deubiquitinase (DUB), and deISGylating (deconjugating interferon-stimulated gene 15 [ISG15] molecule from modified substrates) activities (13–17). In our companion manuscript (18), we describe the X-ray structure-guided identification of a residue in MHV PLP2 that is required for DUB activity, but not protease activity. Using reverse genetics, we generated an MHV that expressed the DUB mutant enzyme, and we found that DUBmut virus is mildly attenuated in mice. However, the role of DUB activity during replication in macrophages, a cell type critical for virus replication and pathogenesis, was not known. We wanted to determine the host response to a DUBmut virus and compare it to that against a virus expressing a mutant form of another recently identified antagonist, the coronavirus endoribonuclease (EndoU).

EndoU, a highly conserved enzyme within the coronavirus family, was initially thought to play a role in coronavirus RNA synthesis (19, 20). Recent studies revealed that EndoU acts as an interferon (IFN) antagonist by preventing activation of host sensors by viral double-stranded RNA (dsRNA) (9, 10). Viruses encoding a catalytically inactive EndoU undergo initial RNA replication; however, viral dsRNA intermediates accumulate during viral replication and are detected by the host sensors MDA5, PKR, and OAS. Activation of these dsRNA sensors initiates the innate immune response, including activation of type I interferons, interferon-responsive genes, and apoptosis-promoting caspases, all of which collectively limit virus replication. We previously reported that MHV-EndoU mutant viruses are profoundly attenuated in mice and elicit a protective immune response (9). In the current study, we use transcriptome profiling to evaluate the kinetics of host gene expression in macrophages upon infection with MHV wild-type (WT), DUBmut, and EndoUmut viruses. Our analyses of the respective transcriptional response to each virus reveal significant differences in the kinetics, magnitude, and breadth of host gene expression during infection and provide new information on the extent to which viral interferon antagonists manipulate the overall host response to viral infection.

RESULTS

Transcriptome profiling reveals differences in kinetics and magnitude of host responses to mutant viruses. We sought to determine if viruses that contain inactivating mutations in distinct interferon antagonists (DUB versus EndoU) would exhibit unique host transcriptional signatures in response to virus infection. Briefly, bone

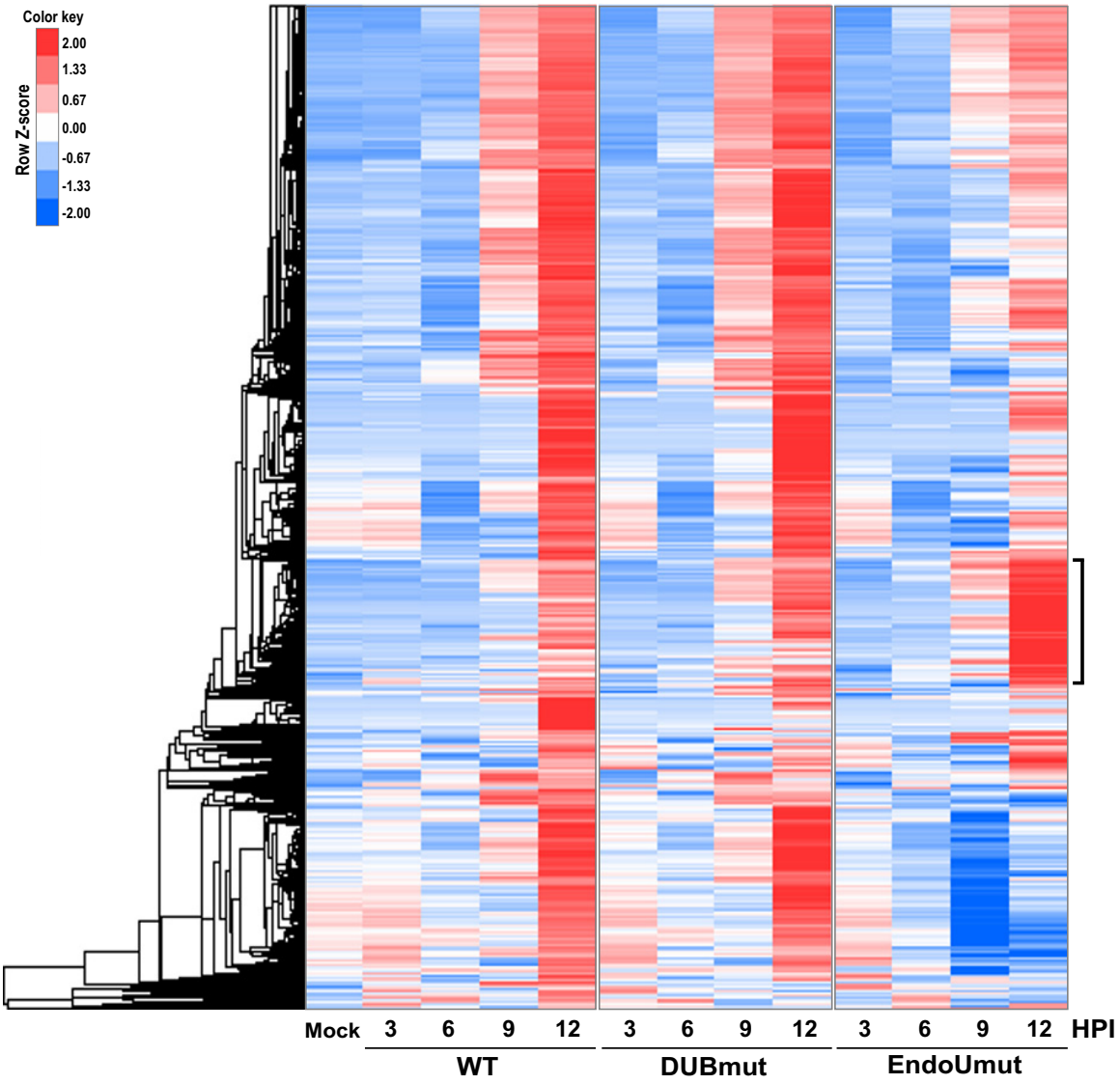

FIG 1 Global gene expression profiles from mock-, WT-, DUBmut-, and EndoUmut-infected BMDMs. Total RNA was extracted from mock- and virus-infected BMDMs at 3, 6, 9, and 12 h postinfection (h p.i.) and sequenced. Raw reads were processed to generate differential expression data and normalized counts. The results are presented as heat maps and line graphs, as described in detail in Materials and Methods. Plotted are row Z-score-standardized $\log_2$-transformed values for each gene across all samples and time points. The colored bar indicates the approximate row Z-score that is associated with each color, with warmer colors corresponding to higher relative expression values within each row and cooler colors corresponding to lower relative expression values. The bracket indicates the genes selected for subsequent analysis in Fig. 2.

marrow-derived macrophages (BMDMs) were infected with the designated virus at a multiplicity of infection (MOI) of 1, and total RNA was harvested for transcriptome profiling at 3, 6, 9, and 12 h postinfection (h p.i.). RNA was isolated from all cells in the well, both infected and uninfected BMDMs. Using the RNA-sequencing (RNA-seq) data, we identified differentially expressed genes by applying a cutoff of at least 4-fold elevated expression in wild-type-infected cells at 12 h p.i. over mock ($q < 0.05$). We then utilized Cluster 3.0 software to visualize overall patterns of gene expression between all groups across all time points (Fig. 1). These analyses reveal striking differences in overall patterns of gene expression between the EndoUmut-infected cells and wild-type virus-infected cells, whereas the gene expression profile induced by the DUBmut virus is remarkably similar to that in wild-type virus infection (Fig. 1). More specifically, 2,879 genes are significantly transcriptionally activated (>4-fold; $q < 0.05$) in WT- and DUBmut-infected macrophages by 12 h p.i. compared to those in mock-infected macrophages. Interestingly,

our analyses also identified a subset of 231 genes, indicated by the bracket in Fig. 1, that were most highly upregulated in EndoUmut-infected cells. It is important to note that these genes were also induced during WT and DUBmut infections, but not to the same magnitude as that detected in the EndoUmut-infected cells. We note a transient downregulation of a subset of genes related to transcriptional responses in the EndoUmut-infected cells at 9 h p.i., which may be related to the apoptotic response of these cells (9). We next sought to functionally cluster the genes most highly upregulated by each mutant virus as a means of investigating the respective host transcriptional response to the different viruses.

EndoUmut infection activates genes associated with an antiviral response. We used an online tool called Database for Annotation, Visualization and Integrated Discovery (DAVID) to cluster the genes highly upregulated by EndoUmut virus infection (bracket in Fig. 1) based on functional similarities (21, 22). We found that the protein products of these genes are predominantly involved in antiviral response and signaling pathways. Notably, the DAVID analyses reveal a subset of 30 unique genes, including several interferon isoforms, which are clustered together into statistically significant pathways associated with the immune response and signaling cascades. Interestingly, the heat map of these genes reveals a similar temporal trend in upregulation of IFN gene expression during infection with each of the three viruses; however, this expression profile is by far the most pronounced in the EndoUmut-infected cells (Fig. 2A). In this heat map view, as in Fig. 1, it is difficult to ascertain any difference in expression of IFN genes between wild-type- and DUBmut-infected cells. Therefore, to obtain more information on the kinetics of transcriptional activation between groups, we quantitated the reads associated with each gene and graphically displayed the normalized read counts (Fig. 2B). Using this method of plotting the read counts over time, we detected statistically significant transcriptional upregulation of IFN gene expression in the DUBmut-infected cells. However, the magnitude of DUBmut-induced IFN gene expression was dwarfed by IFN activation in EndoUmut-infected cells. EndoUmut-infected macrophages exhibited markedly elevated levels of IFN transcripts as early as 9 h p.i. By 12 h p.i., expression of the IFN gene transcripts upon EndoUmut infection was significantly higher than that during wild-type or DUBmut infection, with our assay detecting 1,000 to 10,000 more reads per gene in the EndoUmut-infected cells. This focused response to EndoUmut is successful in limiting virus replication in cultured macrophages, as demonstrated in our previous report (9). Notably, we evaluated the transcriptional response during the first 12 h p.i., prior to the onset of apoptosis, which we and others have shown to occur in BMDMs upon EndoUmut infection (9, 10). We note that the differential expression of IFN genes in the EndoUmut-infected cells influence the row Z-score in Fig. 2A To directly compare IFN gene expression between wild-type and DUBmut infections, we generated a heat map of the comparative response of 15 type I IFNs, with the row Z-score calculations reflecting the relative expression between these two infections (Fig. 2C). Overall, we observe a significant increase in expression of all of these IFNs, particularly at 9 h p.i., during DUBmut-infection relative to that during WT-virus infection. Interestingly, despite of this elevated IFN expression during DUBmut infection, we did not observe a similar increase in ISG15 mRNA, which is upregulated by EndoUmut virus infection (Fig. 2B).

DUBmut-infected cells exhibit downregulation of proinflammatory cytokine and chemokine genes compared to wild-type virus-infected cells. Although we observed an enhanced IFN response during DUBmut infection of BMDMs, this phenotype did not lead to dramatic differences in pathogenesis during infection of mice (18). To further investigate the differences between the host responses to DUBmut versus wild-type virus infection, we reduced the cutoff stringency to at least 2-fold differential expression with a significant q value ($q < 0.05$) and a normalized read count of at least 50. We identified 19 genes upregulated in DUBmut-infected cells at 9 and 12 h p.i. compared to wild type-infected cells (Fig. 3A) and 13 genes downregulated in DUBmut-

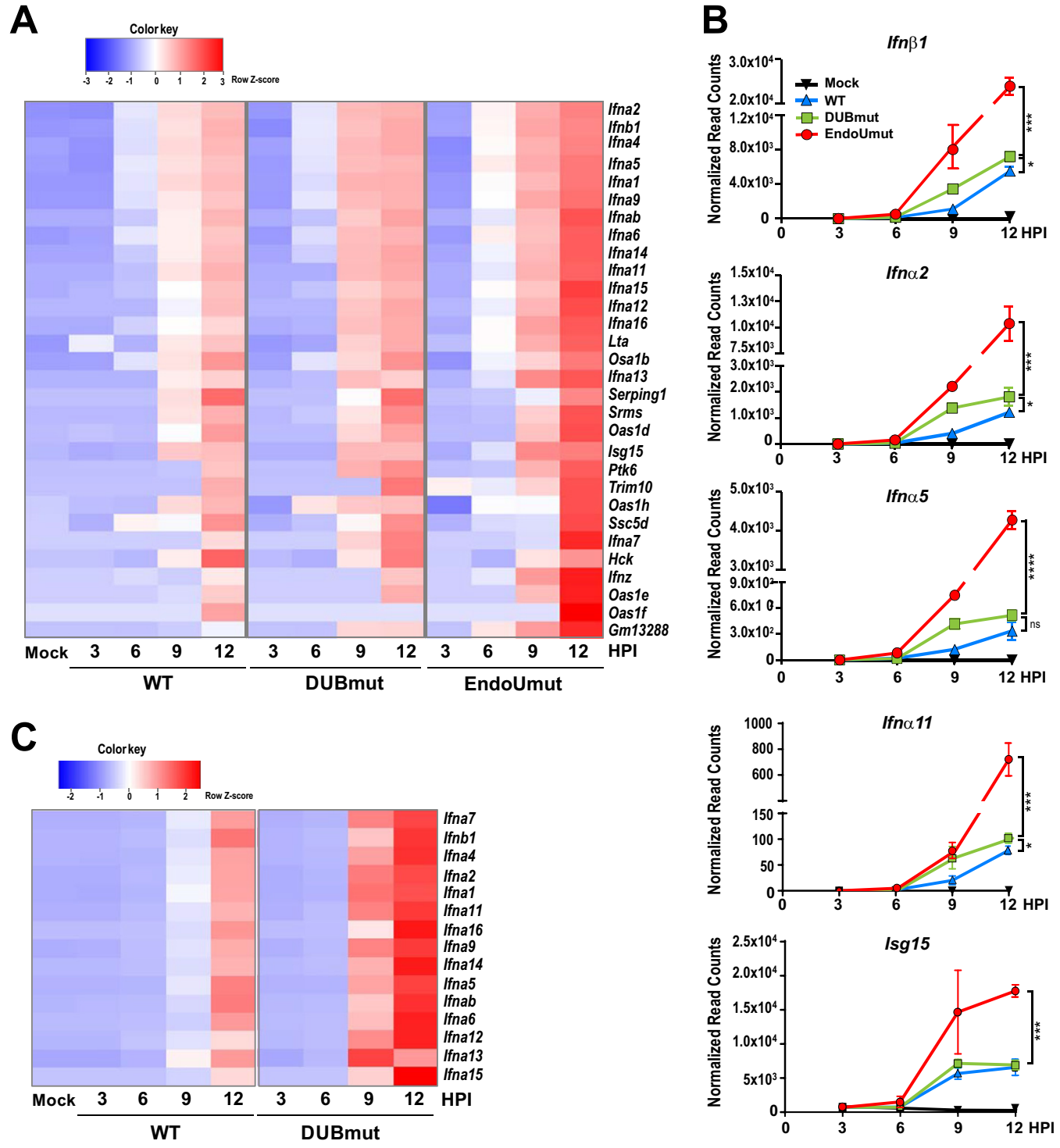

FIG 2 Expression profiles of differentially expressed, functionally clustered genes (DAVID). The expression profiles of the genes within the cluster bracketed in Fig. 1 were analyzed using DAVID. The 30 genes that were grouped by DAVID into statistically significant functional clusters are plotted as a heat map, as described in Materials and Methods. Plotted are row Z-score-standardized $\log_2$-transformed means of replicates for all samples. (A) Expression profiles of WT, DUBmut, and EndoUmut infections for type I interferons and interferon-stimulated genes (ISGs) that were clustered by DAVID analysis. (B) Line graphs of normalized read count values for select genes. Plotted are the average normalized counts for each gene over all four time points. (C) Expression profile of WT and DUBmut infections for type I interferons. The normalized counts from each infection group at 12 h postinfection (h p.i.) were subjected to statistical testing using two-tailed Student's *t* tests. *, $P < 0.05$; **, $P < 0.01$; ***, $P < 0.001$; ****, $p < 0.0001$; ns, not significant. Data are presented as means ± standard deviation (SD).

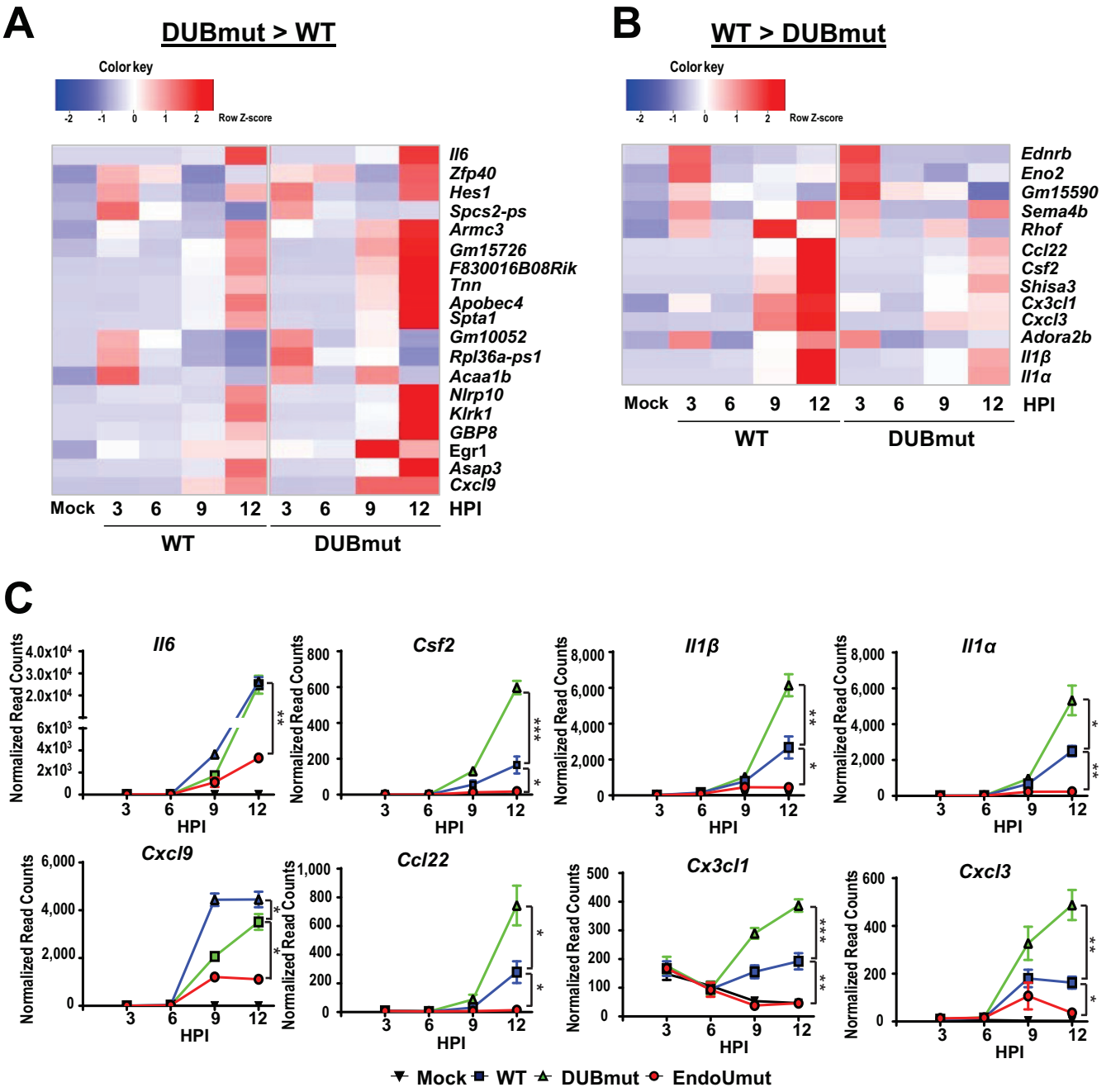

FIG 3 Differential expression profiles of DUBmut- versus WT-infected BMDMs. Differential gene expression analyses were performed on DUBmut- and WT-infected samples. A statistically significant q value of < 0.05 and a fold change cutoff of >2 were applied. (A and B) Expression profiles for genes that were differentially expressed at 9 h p.i. or 12 h p.i. with (A) increased gene expression during DUBmut infection or (B) decreased expression during DUBmut infection compared to that during WT infection. (C) Line graphs of normalized read count values for selected genes. Plotted are the average normalized counts for each gene in EndoUmut- (red), DUBmut- (green), WT MHV- (blue), and mock-infected (black) BMDM infection groups over all 4 time points. The normalized counts from each infection group at 12 h postinfection (h p.i.) were subjected to statistical testing using two-tailed Student's t tests. *, $P < 0.05$; **, $P < 0.01$; ***, $P < 0.001$; ****, $p < 0.0001$; ns, not significant. Data are presented as means ± SD.

infected cells compared to WT-infected cells (Fig. 3B). Our analysis identified dysregulation relative to the wild type of multiple genes that encode proinflammatory cytokines and chemokines, including *Il6*, *Il1β*, and *Il1α* (Fig. 3C). Interestingly, wild type-infected cells exhibited the highest levels of expression for most of these cytokines, while DUBmut-infected cells were characterized by decreased expression of *Csf2*, *Il1β*, and *IL1α*. DUBmut virus infection induced upregulation of *Cxcl9*, but downregulation of

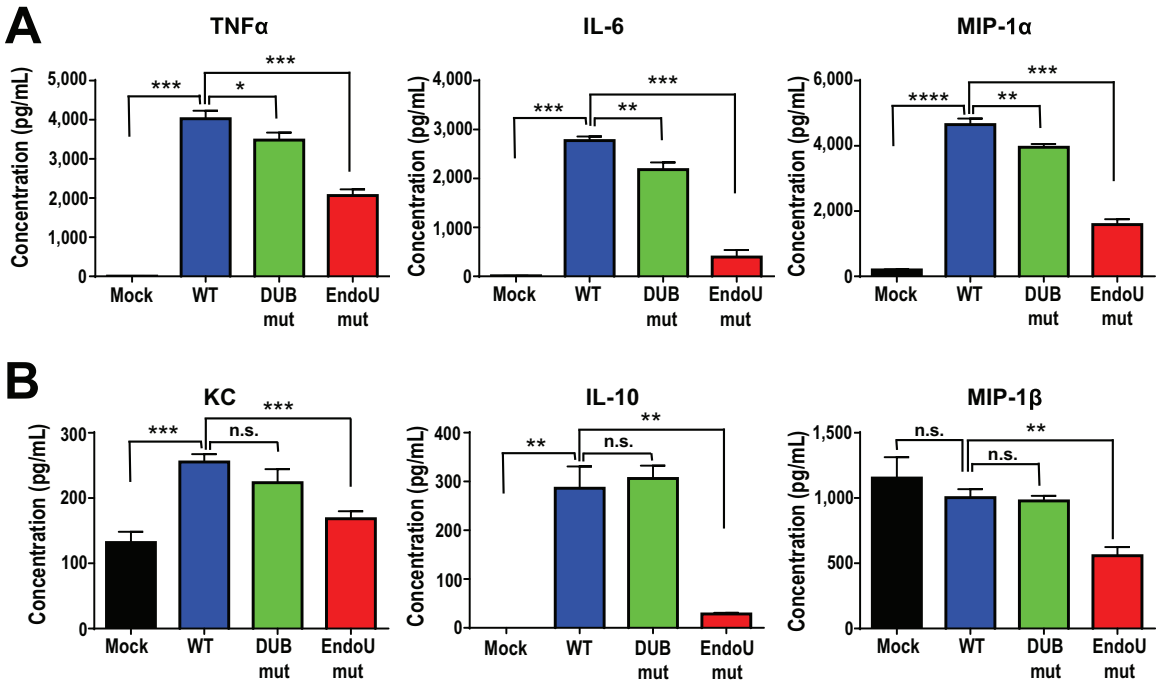

FIG 4 Differential proinflammatory cytokine profiles during WT, DUBmut, and EndoUmut infections. BMDMs were infected with WT-, DUBmut-, or EndoUmut-MHV at an MOI of 1. At 24 h p.i., cell-free supernatants were collected, and cytometric bead array analysis was performed for the selected pro- and anti-inflammatory cytokines and chemokines. (A) Supernatant protein concentrations of cytokines differentially secreted during DUBmut or EndoUmut infections compared to those during WT infection. (B) Supernatant protein concentrations of cytokines differentially secreted during EndoUmut infections only compared to those secreted during DUBmut and WT infections. The following cytokines were analyzed but not shown because we detected no significance compared to mock infections: IL-1α, IL-1β, IL-2, IL-17a, IFN-γ, IL-13, MCP-1, and IL-4. Data were subjected to statistical analysis using two-tailed Student's *t* tests. *, $P < 0.05$; **, $P < 0.01$; ***, $P < 0.001$; ****, $P < 0.0001$; ns, not significant. Data are presented as means ± SD.

Ccl22, *Cx3cl1*, and *Cxcl3*, compared to WT-infected cells. We note that the host response to wild-type and DUBmut virus infections trended in the same direction and that these cytokine and chemokine responses were much more robust compared to the response to the EndoUmut virus infection.

The results of proinflammatory cytokines gene expression shown in Fig. 3 prompted us to evaluate secretion of proinflammatory cytokines in response to the wild-type, DUBmut, and EndoUmut virus infection. To determine the concentrations of pro- and anti-inflammatory cytokines released during infection, we performed cytometric bead array (CBA) analysis on supernatants collected from virus-infected BMDMs at 24 h p.i. We performed the CBA at 24 h p.i. to allow for the cytokine mRNA to be translated into protein and the protein to be secreted from the cells into the supernatant. We report that DUBmut- and EndoUmut-infected cells have reduced levels of the inflammatory cytokines tumor necrosis factor alpha (TNF-α), interleukin 6 (IL-6), and macrophage inflammatory protein 1α (MIP-1α) relative to those in wild-+ type-infected cells (Fig. 4A). We also found that EndoUmut-infected cells exhibit lower levels of KC, IL-10, and MIP-1β proteins relative to those in WT- and DUBmut-infected cells (Fig. 4B). EndoUmut viruses induce apoptosis in BMDMs (9), which likely limits their ability to produce proinflammatory cytokines. The results of these analyses indicate that wild type-infected BMDMs have a heightened proinflammatory profile compared to those of DUBmut- and EndoUmut-infected cells. This proinflammatory cytokine response has been shown to contribute to increased immunopathogenesis during *in vivo* infections (23).

Wild-type and DUBmut coronavirus replication activate the unfolded protein response and host response to cell damage. In contrast to the robust and specific antiviral gene expression response detected in EndoUmut-infected macrophages, we uncovered a more complex response involving 2,879 genes in both wild-type- and

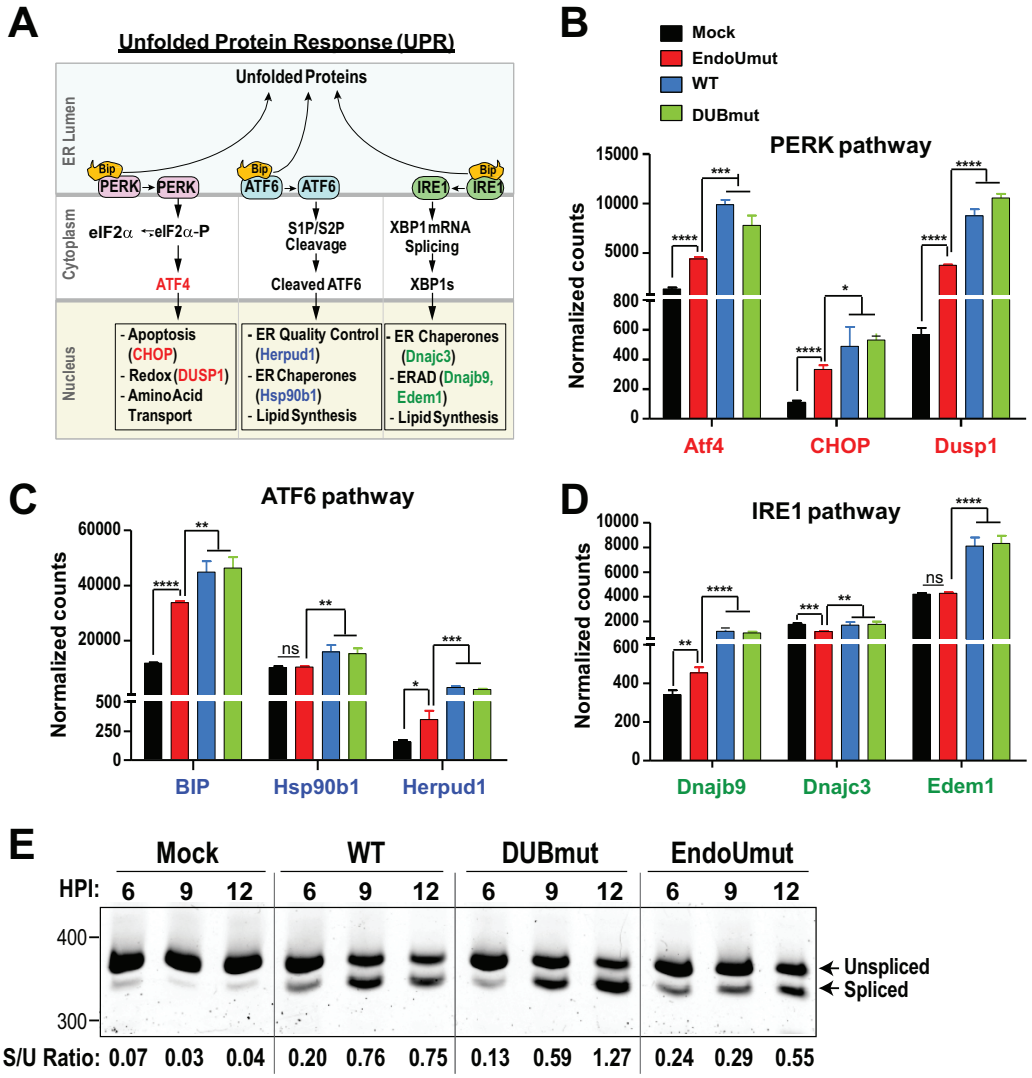

FIG 5 Expression of genes implicated in UPR pathways in WT-, DUBmut-, and EndoUmut-infected BMDMs at 12 h p.i. (A) Schematic diagram of unfolded protein response. To evaluate the transcriptional response during viral infection, normalized count values for nine UPR-induced genes at 12 h p.i. are plotted. Genes are grouped into three panels according to whether their expression is triggered by (B) PERK, (C) ATF6, or (D) IRE1 pathway signaling. (E) PCR analysis of XBP1 splicing. The ratio was calculated for each lane by dividing the density of the spliced band by the density of the unspliced band. Data were subjected to statistical analysis using two-tailed Student's *t* tests. *, $P < 0.05$; **, $P < 0.01$; ***, $P < 0.001$; ****, $P < 0.0001$; ns, not significant. Data are presented as means ± SD.

DUBmut virus-infected macrophages by 12 h p.i. The overall patterns of expression of these genes in DUBmut- and WT-infected BMDMs are strikingly similar by 12 h p.i. (Fig. 1 and 2). In addition to a similar proinflammatory signature (Fig. 3 and 4), we found that wild type- and DUBmut-infected cells also exhibit hallmarks of activation of the host unfolded protein response (UPR).

UPR pathways are activated when unfolded proteins accumulate in the endoplasmic reticulum (ER), at which point the host cell initiates measures to resolve this overload (24). In the context of virus infection, viral glycoproteins accumulate in the ER, triggering the release of BiP from three sensor proteins: IRE1, ATF6, and PERK. Activation of these sensors triggers signaling cascades resulting in transcriptional activation of genes encoding ER chaperones and proteins involved in lipid synthesis and amino acid transport (Fig. 5A). Our previous study documented the activation of these pathways after MHV infection of fibroblasts (25). This study provides new information on the early transcriptional response to MHV in macrophages. Based on our analyses of differential

gene expression, we report significant transcriptional upregulation of multiple genes associated with activation of ER sensors IRE1, ATF6, and PERK, such as *Edem1*, *Hspa5* (encoding BiP protein), and *Ddit3* (encoding CHOP), in response to virus replication, with the most robust response detected in cells infected with the wild-type or DUBmut virus infection (Fig. 5B, C, and D). To further evaluate the activation of IRE-1 during virus infection, we analyzed the splicing of XBP-1 mRNA by reverse transcription-PCR (RT-PCR) and visualized the products by electrophoresis on agarose gels. We found that the WT and DUBmut viruses exhibit higher proportions of spliced XBP-1 mRNA at 9 h p.i. and 12 h p.i. compared to that in EndoUmut-infected cells (Fig. 5E), consistent with activation of the IRE-1 arm of the unfolded protein response. Overall, these differential gene expression analyses in macrophages reveal similar host responses to the wild-type and DUBmut viruses that include activation of UPR pathways and proinflammatory genes, whereas a distinct transcriptional profile during infection with the EndoUmut virus is predominately defined by a focused, robust antiviral response.

DISCUSSION

We report that inactivation of a coronaviral interferon antagonist, EndoU, profoundly alters the host response to viral replication in macrophages compared to the response to wild-type coronavirus infection. We find that the EndoUmut virus elicits a rapid, robust, and specific antiviral response that is effective in limiting virus replication. In contrast, our data show that the wild-type and DUBmut viruses ultimately elicit very similar host responses that are both characteristic of an unfolded protein response and consistent with a proinflammatory profile that is associated with viral pathogenesis (23). Our studies of the DUBmut-infected macrophages indicate that mere induction of type I IFN is not a sufficient marker for attenuation of the virus. Instead, these results suggest that the timing and the magnitude of the host antiviral response are critical for determining the outcome of infection in macrophages (Fig. 6) and for pathogenesis in infected animal (18). Our observation that the EndoUmut virus induces an earlier and more profoundly elevated type I interferon response than even the DUBmut virus implies that there is a threshold of IFN expression that must be breached before the cell mounts an effective antiviral response.

A remarkable finding from this study is the distinct transcriptional profile elicited by the EndoUmut virus during infection of bone marrow-derived macrophages compared to the profiles of wild-type- and DUBmut-infected cells (Fig. 1). We detected elevated levels of interferon and interferon-responsive genes as early as 6 to 9 h p.i., with EndoUmut-infected cells exhibiting by far the highest expression levels of these genes. We and others found that an antiviral response to EndoUmut infection results in activation of apoptosis, which subsequently limits virus replication in cell culture and in infected mice (9, 10). The current study indicates that screening MHV mutants in interferon-responsive cells may be an effective approach to identifying mutations that stimulate a robust innate immune response, which may then restrict virus replication in animals. Previous studies of coronavirus-encoded interferon antagonists focused on evaluating the host transcriptional response to infection at later time points (such as 24 and 48 h p.i.) and in a variety of cell types or the tissues of infected animals. For example, a study comparing infection of mice with wild-type SARS-CoV versus a virus containing a mutation in the interferon antagonist nsp16, termed the dNSP16 CoV, revealed that the transcriptional profile in the lungs of the dNSP16-infected mice mirrored the response to WT virus (11). However, combining the dNSP16 mutation with a mutation in another interferon antagonist, ExoN, was shown to reduce disease in mice and elicit protective immunity. It would be interesting to determine if the transcriptional profile elicited by the double mutant SARS-CoV is altered compared to that of the wild-type virus, particularly at early times after infection. A study of MERS-CoV comparing the host response to WT virus with the response to a mutant virus containing deleted accessory open reading frames (ORFs) (MERS-CoV dORF3-5) provides evidence of significant differences in the early transcriptional responses to

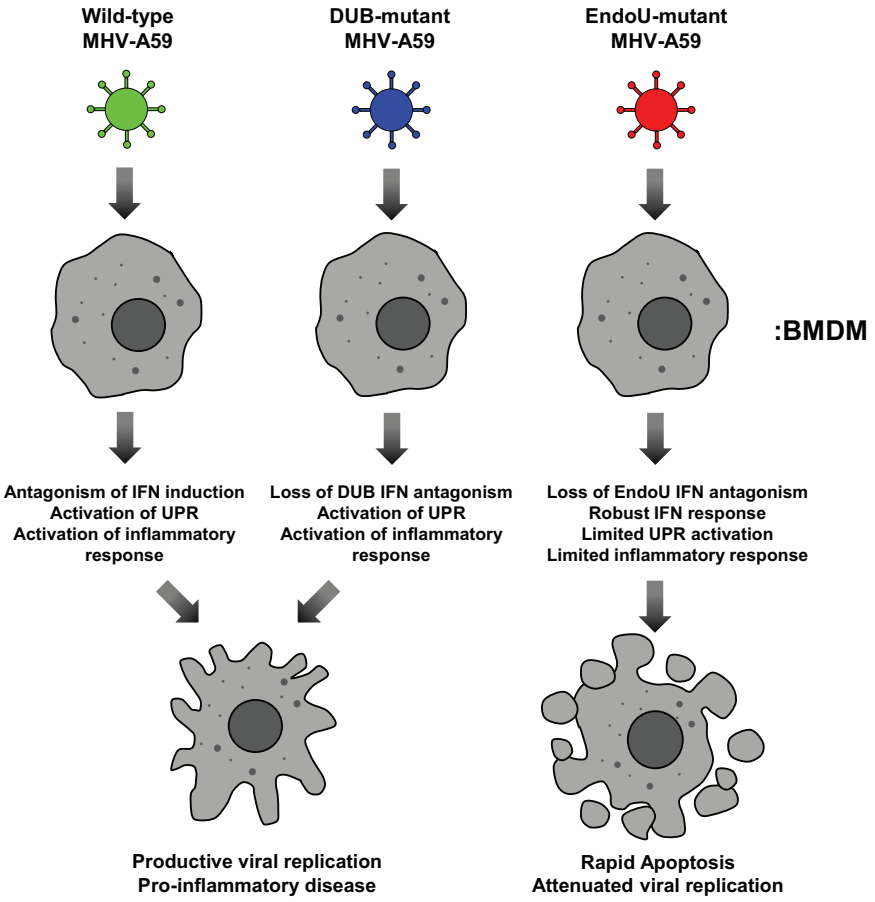

FIG 6 Proposed model for outcomes of WT-MHV, DUBmut-MHV, and EndoUmut-MHV infection of BMDMs. Upon infection of a BMDM with EndoUmut, host double-stranded RNA (dsRNA) sensors (including MDA5, PKR, and OAS) are activated, resulting in robust transcription of type I IFN genes and rapid induction of apoptosis, the latter of which precludes the development of a potent inflammatory response. Viral replication is severely restricted in these apoptotic macrophages as early as 6 h p.i. Although DUBmut induces significantly higher type I IFN during infection than WT-MHV, infection with either DUBmut or the WT yields same outcome, accumulation of ER stress and subsequent activation of the UPR, which then likely leads to the establishment of a robust NF-κB-mediated proinflammatory response. BMDMs infected with either of these viruses acquire a potently activated inflammatory phenotype, are unable to attenuate viral replication, and likely contribute to severe immunopathology *in vivo*.

infection in Calu3 2B4 cells (26). This study revealed that MERS-CoV dORF3-5 infection prompted earlier (7, 12, and 24 h p.i.) and more robust type I and type III interferon responses, and that the mutant virus was more sensitive than the wild type to pretreatment with interferon. The MERS-CoV interferon antagonist mutant virus was attenuated in mice and elicited a protective response against subsequent lethal challenge.

One difficulty that arises when evaluating the role(s) of virally mediated modulation of the host response is that multiple viral proteins, including both structural and nonstructural proteins, have been shown to antagonize the innate immune response *in vitro* and/or *in vivo*. These include: nsp16-2′O MTase, nsp14-ExoN, nsp1, nsp7, E protein, N protein, M protein, SARS-CoV-ORF6, MERS-CoV-ORF3-5, MERS-CoV-4a, and MERS-CoV-4b (11, 26–30). Each of these interferon antagonists may play either a cell- or tissue-type-specific role, or may act in concert with other factors during viral replication to mitigate the innate immune response. Further studies are needed to fully understand if all or only a subset of these antagonists must be silenced to generate an effective live-attenuated vaccine. The results presented here, and from studies of the MERS-CoV dORF3-5 mutant virus (26), inactivating nsp14 and nsp16 of SARS-CoV (11)

and inactivating nsp15 in PEDV (31), suggest that inactivating interferon antagonists and screening for an early and robust antiviral transcriptional profile may represent an efficient and informative approach to evaluating live-attenuated vaccine candidate strains for existing and emerging coronaviruses.

The dysregulation of innate immune signaling in myeloid cells, such as macrophages, is a key component of coronavirus-associated immunopathogenesis (32–34). Using viral infection of macrophages, we can identify and evaluate the viral factors involved in antagonizing innate immune pathways. We and others have found that EndoU is important for the inhibition of innate immune signaling in macrophages (9, 10). Loss of EndoU activity significantly alters gene expression and cytokine production in macrophages, which results in the attenuation of EndoUmut viruses *in vivo* (9). In contrast, we report mild attenuation of the DUBmut virus in mice (18) and show here that DUBmut and MHV-A59 generate similar patterns of transcriptional activation in macrophages. While macrophages have been documented to be important for controlling CoV infections, it is also important to appreciate that CoVs infect multiple cell types, including as epithelial cells in the lung and intestines. Viral DUB activity may play a more significant role during infection of epithelial cells, and further studies are needed to provide further insights into the role of DUB activity during coronavirus infection.

Our results demonstrating upregulation of the unfolded protein response (UPR) in response to wild-type and DUBmut coronavirus replication confirm and extend the work of earlier studies that documented activation of the ER sensors PERK, IRE1, and ATF-6 during coronavirus infection (25, 29, 35). Heavy utilization of the endoplasmic reticulum for generating coronavirus replication complexes and of the ER-Golgi intermediate compartment for assembling virus particles places a substantial load on the host translational machinery during infection. Host sensors IRE1, ATF-6, and PERK are situated in the ER to sense and respond to such overload by prompting upregulated expression of genes encoding ER chaperones, amino acid transporters, and activators of lipid biosynthesis. Ultimately, many of these proteins may facilitate virus replication and assembly. Notably, it has been demonstrated that UPR pathways that promote apoptosis are blocked during coronavirus replication (25, 29). The ability of viruses to modulate the UPR has important implications for the innate immune response to such viruses because the UPR has been shown to attenuate antiviral defenses by way of degrading the type I interferon receptor (36). To our knowledge, the data presented here provide the first transcriptomic evidence of UPR activation in coronavirus-infected macrophages, underlining an important role for UPR pathways in the coronavirus life cycle. Our observation that EndoUmut-infected macrophages exhibit significantly lower expression of several genes involved in UPR pathways compared with wild type- and DUBmut-infected cells is consistent with the reduced levels of virus replication detected in EndoUmut-infected macrophages.

The notion of inactivating viral interferon antagonists as a means of generating live-attenuated vaccines is supported by recent reports of screening for inactivation of influenza A virus-encoded interferon antagonists (3), as well as studies that revealed that the classic vaccine strain of yellow fever virus encodes an interferon antagonist in the NS5 protein (37). For coronaviruses, it is not yet clear if disabling a single interferon antagonist, such as the highly conserved EndoU, will be sufficient to attenuate viruses that infect different cell types in different species. Promisingly, our studies of a coronavirus that causes lethal disease in piglets, porcine epidemic diarrhea virus (PEDV), revealed that inactivation of EndoU activity is associated with attenuated disease (31). We believe the information gained from studying coronaviruses containing inactivated interferon antagonists can be directly applied to the recently emerged coronavirus designated severe acute respiratory syndrome coronavirus 2 (SARS-CoV-2) (38–40). More research is needed to determine if inactivating multiple interferon antagonists, including EndoU, is an effective approach for generating safe and protective live-attenuated coronavirus vaccines.

MATERIALS AND METHODS

Ethics statement. The harvesting of bone marrow for obtaining bone marrow-derived macrophages in this study was carried out in accordance with the recommendations in the Guide for the Care and Use of Laboratory Animals of the National Institutes of Health. The experimental protocol was reviewed and approved by the Institutional Animal Care and Use Committee (IACUC) at Loyola University Chicago (IACUC no.2016-029). C57BL/6 female mice were purchased from The Jackson Laboratory and maintained in the Comparative Medicine Facility of Loyola University Chicago.

BMDMs and viruses. Bone marrow-derived macrophages (BMDMs) were prepared and cultured as described previously (9). Differentiated BMDMs were maintained in bone marrow macrophage (BMM) media containing Dulbecco's modified Eagle's medium (DMEM) (product no. 10-017-CV; Corning) supplemented with 30% L929 cell supernatant, 20% fetal bovine serum (FBS), 1% L-glutamine, 1% sodium pyruvate, and 1% penicillin-streptomycin. Wild-type MHV strain A59 (GenBank accession number AY910861) and EndoUmut (H262A) were previously generated by reverse genetics and confirmed by deep sequencing. DUBmut (D1772A) was generated as described in the companion paper (18).

RNA-seq data analysis pipeline. RNA-seq data have been deposited in the NCBI GEO database (accession number GSE144882). Raw RNA-seq reads were subjected to analysis using Galaxy's online platform to generate differential gene expression data between infection groups (41). Reads were clipped to remove any residual unique barcode sequences that were added during preparation of each sample for sequencing. Clipped reads were concatenated to combine multiple files per sample into a single file per sample. These files were groomed to ensure that all reads were in Sanger FASTQ format. FASTQ reads were aligned to the GRCm38 Ensembl build of the C57BL/6J mouse genome using the HISAT2 aligner, which locates the region of the genome to which each read corresponds, resulting in an output BAM file (42). All reads that did not align to the mouse genome (i.e., reads that originated from viral RNA) were discarded. The BAM files contained the alignment information for each read in that sample and were used as inputs into featureCounts, which quantifies the number of reads in each sample that corresponds to each gene in the mouse genome (43). Finally, the output count data from featureCounts was used as the input for DESeq2 to calculate differential expression for each gene across all samples and treatment groups. DESeq2 was used to generate normalized count values for each gene in all samples (44). These normalized counts are intended to correct for size differences between samples that might otherwise skew differential expression calculations if some samples contained substantially different numbers of total reads. The normalized count values were plotted and visualized in heat maps, generated using R, and line graphs, generated using Prism software.

Identifying differentially expressed genes. To identify and analyze differentially expressed genes (DEGs) between infection groups, we used as a starting point the list of DEGs between mock- and wild-type MHV-infected BMDMs at 12 h p.i. that was generated as an output by DESeq2. This list of genes was filtered based on the statistical significance associated with the fold change differential expression value. A q value (adjusted P value, calculated by DESeq2 for each gene in each comparison using the Benjamini-Hochberg procedure) of <0.05 was chosen as the cutoff for statistical significance; genes whose differential upregulation values did not meet this cutoff in wild-type MHV-infected BMDMs at 12 h p.i. compared with mock-infected cells were removed from the list (44). Next, a differential expression magnitude cutoff of >4 was applied to the remaining genes. Genes that were not more highly expressed by at least 4-fold in wild-type MHV-infected cells at 12 h p.i. compared to mock were removed from the list. After applying these cutoffs, 2,879 genes remained and were arranged in order of most to least highly upregulated in wild-type MHV-infected cells at 12 h p.i. compared to mock. Cluster 3.0 software was then used to apply mathematical clustering to the Z-score-standardized $\log_2$-normalized mean normalized count values associated with each gene at each time point and in each infection group (45). Specifically, the default settings—the similarity metric "Pearson correlation (uncentered)" and the clustering method "centroid linkage"—were applied to the list of 2,879 genes and the corresponding expression values for each gene across all samples to produce a hierarchically clustered gene list based on how similar or different the expression patterns were between groups of genes across all samples. This new list of clustered genes and their associated expression values were then visualized as a heat map using Java TreeView software.

Functional clustering analyses using DAVID. The bracketed set of 231 genes identified in Fig. 1 were subjected to DAVID analyses. Specifically, under the "Gene Ontology" category, the data from the chart associated with the "GOTERM_BP_DIRECT" result were reported here. After excluding all functional cluster terms that were not statistically significant using a cutoff of $q < 0.05$, we identified a total of 30 unique genes that appeared in at least one cluster of statistical significance. Expression values of these genes were plotted in heat map and line graph forms as described above.

XBP-1 splice analysis. C57BL/6 BMDMs were infected with wild-type-, DUBmut-, or EndoUmut-MHV at an MOI of 1. At designated time points, intracellular RNA was isolated from cells with RNeasy kit (catalog no. 74104; Qiagen). Isolated RNA was reverse transcribed into cDNA with an RT² First Strand kit (catalog no. 330411; Qiagen). XBP-1 splicing was analyzed by PCR following the protocol from Bechill et al. (25). Briefly, PCR was performed with the forward primer 5′-GTTGAGAACCAGGAGTTAAG-3′ and the reverse primer, 5′-AGAGAAAGGGAGGCTGGTAAG-3′. PCR conditions were (i) 95°C for 2 min, (ii) 95°C for 1 min, (iii) 58°C for 1 min, and (iv) 72°C for 1 min, repeating steps ii to iv for 40 cycles. PCR products were separated on 5% polyacrylamide-TBE (20 mM Tris-borate and 0.5 mM EDTA [pH 8.0]) gel, stained with SYBR green II stain, and imaged. Quantification of band density was performed with Image Lab software (Bio-Rad).

Cytometric bead array. C57BL/6 BMDMs were infected with wild-type-, DUBmut-, or EndoUmut-MHV at an MOI of 1. At 24 h p.i., supernatants were collected and centrifuged at 1,000 $\times$ g for 5 min at

4°C to remove cellular debris. CBA staining was performed according to the manufacturer's instructions (CBA Flex Set mouse soluble proteins, catalog no. 558266; BD Biosciences). Bead fluorescence was measured with an LSR Fortessa cell analyzer (BD Biosciences), and data were analyzed using FCAP Array software 3.0 (BD Biosciences).

ACKNOWLEDGMENTS

We thank Qunfeng Dong for assistance with the bioinformatic analyses. We also thank Robert Mettelman for assistance with quantitative PCR (qPCR) setups and help editing the manuscript. We thank Francis Alonzo III and Zack Resko for assistance with the cytometric bead array analyses.

This work was supported by National Institutes of Health (NIH) grant R01 AI085089 (to S.C.B.). M.H. was supported by NIH T32 Training Grant for Experimental Immunology (no. AI007508).

Conceptualization: A.V., M.H., and S.C.B. Investigation: A.V., M.H., and Y.C.-P. Formal Analysis: A.V., M.H., X.D., and S.C.B. Writing – Original Draft Preparation: A.V., M.H., and S.C.B. Writing – Review & Editing, with comments from: A.V., M.H., X.D., Y.C.-P., A.O., and S.C.B. Visualization: A.V., M.H., A.O., and S.C.B. Funding Acquisition and Supervision: S.C.B.

REFERENCES

1. Chatterjee S, Basler CF, Amarasinghe GK, Leung DW. 2016. Molecular mechanisms of innate immune inhibition by non-segmented negative-sense RNA viruses. J Mol Biol 428:3467–3482. https://doi.org/10.1016/j.jmb.2016.07.017.
2. Stuart JH, Sumner RP, Lu Y, Snowden JS, Smith GL. 2016. *Vaccinia* virus protein C6 inhibits type I IFN signalling in the nucleus and binds to the transactivation domain of STAT2. PLoS Pathog 12:e1005955-24. https://doi.org/10.1371/journal.ppat.1005955.
3. Du Y, Shi Y, Zhang T-H, Dai L, Gong D, Brar G, Shu S, Luo J, Tseng Y-W, Wu T-T, Wang J, Sun R, Xin L, Bai H, Shu Y, Wu NC, Reiley W. 2018. Genome-wide identification of interferon-sensitive mutations enables influenza vaccine design. Science 359:290–296. https://doi.org/10.1126/science.aan8806.
4. Best SM. 2017. The many faces of the flavivirus NS5 protein in antagonism of type I interferon signaling. J Virol 91:e01970-16. https://doi.org/10.1128/JVI.01970-16.
5. Kindler E, Thiel V. 2014. To sense or not to sense viral RNA-essentials of coronavirus innate immune evasion. Curr Opin Microbiol 20:69–75. https://doi.org/10.1016/j.mib.2014.05.005.
6. Perlman S, Netland J. 2009. Coronaviruses post-SARS: update on replication and pathogenesis. Nat Rev Microbiol 7:439–450. https://doi.org/10.1038/nrmicro2147.
7. Cui J, Li F, Shi Z-L. 2019. Origin and evolution of pathogenic coronaviruses. Nat Rev Microbiol 17:181–192. https://doi.org/10.1038/s41579-018-0118-9.
8. Niemeyer D, Mösbauer K, Klein EM, Sieberg A, Mettelman RC, Mielech AM, Dijkman R, Baker SC, Drosten C, Müller MA. 2018. The papain-like protease determines a virulence trait that varies among members of the SARS-coronavirus species. PLoS Pathog 14:e1007296. https://doi.org/10.1371/journal.ppat.1007296.
9. Deng X, Hackbart M, Mettelman RC, O'Brien A, Mielech AM, Yi G, Kao CC, Baker SC. 2017. Coronavirus nonstructural protein 15 mediates evasion of dsRNA sensors and limits apoptosis in macrophages. Proc Natl Acad Sci U S A 114:E4251–E4260. https://doi.org/10.1073/pnas.1618310114.
10. Kindler E, Gil-Cruz C, Spanier J, Li Y, Wilhelm J, Rabouw HH, Züst R, Hwang M, V'kovski P, Stalder H, Marti S, Habjan M, Cervantes-Barragan L, Elliot R, Karl N, Gaughan C, van Kuppeveld FJM, Silverman RH, Keller M, Ludewig B, Bergmann CC, Ziebuhr J, Weiss SR, Kalinke U, Thiel V. 2017. Early endonuclease-mediated evasion of RNA sensing ensures efficient coronavirus replication. PLoS Pathog 13:e1006195. https://doi.org/10.1371/journal.ppat.1006195.
11. Menachery VD, Gralinski LE, Mitchell HD, Dinnon KH, Leist SR, Yount BL, McAnarney ET, Graham RL, Waters KM, Baric RS. 2018. Combination attenuation offers strategy for live-attenuated coronavirus vaccines. J Virol 92:e00710-18. https://doi.org/10.1128/JVI.00710-18.
12. Totura AL, Baric RS. 2012. SARS coronavirus pathogenesis: host innate immune responses and viral antagonism of interferon. Curr Opin Virol 2:264–275. https://doi.org/10.1016/j.coviro.2012.04.004.
13. Barretto N, Jukneliene D, Ratia K, Chen Z, Mesecar AD, Baker SC. 2005. The papain-like protease of severe acute respiratory syndrome coronavirus has deubiquitinating activity. J Virol 79:15189–15198. https://doi.org/10.1128/JVI.79.24.15189-15198.2005.
14. Lindner HA, Fotouhi-Ardakani N, Lytvyn V, Lachance P, Sulea T, Ménard R. 2005. The papain-like protease from the severe acute respiratory syndrome coronavirus is a deubiquitinating enzyme. J Virol 79:15199–15208. https://doi.org/10.1128/JVI.79.24.15199-15208.2005.
15. Ratia K, Saikatendu KS, Santarsiero BD, Barretto N, Baker SC, Stevens RC, Mesecar AD. 2006. Severe acute respiratory syndrome coronavirus papain-like protease: structure of a viral deubiquitinating enzyme. Proc Natl Acad Sci U S A 103:5717–5722. https://doi.org/10.1073/pnas.0510851103.
16. Ratia K, Kilianski A, Baez-Santos YM, Baker SC, Mesecar A. 2014. Structural basis for the ubiquitin-linkage specificity and deISGylating activity of SARS-CoV papain-like protease. PLoS Pathog 10:e1004113. https://doi.org/10.1371/journal.ppat.1004113.
17. Mielech AM, Kilianski A, Baez-Santos YM, Mesecar AD, Baker SC. 2014. MERS-CoV papain-like protease has deISGylating and deubiquitinating activities. Virology 450–451:64–70. https://doi.org/10.1016/j.virol.2013.11.040.
18. Deng X, Chen Y, Mielech AM, Hackbart M, Kesely KR, Mettelman RC, O'Brien A, Chapman ME, Mesecar AD, Baker SC. 2020. Structure-guided mutagenesis alters deubiquitinating activity and attenuates pathogenesis of a murine coronavirus. J Virol 94:e01734-19. https://doi.org/10.1128/JVI.01734-19.
19. Snijder EJ, Bredenbeek PJ, Dobbe JC, Thiel V, Ziebuhr J, Poon LLM, Guan Y, Rozanov M, Spaan WJM, Gorbalenya AE. 2003. Unique and conserved features of genome and proteome of SARS-coronavirus, an early split-off from the coronavirus group 2 lineage. J Mol Biol 331:991–1004. https://doi.org/10.1016/S0022-2836(03)00865-9.
20. Ivanov KA, Hertzig T, Rozanov M, Bayer S, Thiel V, Gorbalenya AE, Ziebuhr J. 2004. Major genetic marker of nidoviruses encodes a replicative endoribonuclease. Proc Natl Acad Sci U S A 101:12694–12699. https://doi.org/10.1073/pnas.0403127101.
21. Huang DW, Sherman BT, Lempicki RA. 2009. Bioinformatics enrichment tools: paths toward the comprehensive functional analysis of large gene lists. Nucleic Acids Res 37:1–13. https://doi.org/10.1093/nar/gkn923.
22. Huang DW, Sherman BT, Lempicki RA. 2009. Systematic and integrative analysis of large gene lists using DAVID bioinformatics resources. Nat Protoc 4:44–57. https://doi.org/10.1038/nprot.2008.211.
23. Channappanavar R, Fehr AR, Vijay R, Mack M, Zhao J, Meyerholz DK, Perlman S. 2016. Dysregulated type I interferon and inflammatory monocyte-macrophage responses cause lethal pneumonia in SARS-CoV-infected mice. Cell Host Microbe 19:181–193. https://doi.org/10.1016/j.chom.2016.01.007.
24. Grootjans J, Kaser A, Kaufman RJ, Blumberg RS. 2016. The unfolded protein response in immunity and inflammation. Nat Rev Immunol 16:469–484. https://doi.org/10.1038/nri.2016.62.
25. Bechill J, Chen Z, Brewer JW, Baker SC. 2008. Coronavirus infection

modulates the unfolded protein response and mediates sustained translational repression. J Virol 82:4492–4501. https://doi.org/10.1128/JVI.00017-08.
26. Menachery VD, Mitchell HD, Cockrell AS, Gralinski LE, Yount BL, Graham RL, McAnarney ET, Douglas MG, Scobey T, Beall A, Dinnon K, Kocher JF, Hale AE, Stratton KG, Waters KM, Baric RS. 2017. MERS-CoV accessory ORFs play key role for infection and pathogenesis. mBio 8:e00665-17. https://doi.org/10.1128/mBio.00665-17.
27. Frieman M, Yount B, Heise M, Kopecky-Bromberg SA, Palese P, Baric RS. 2007. Severe acute respiratory syndrome coronavirus ORF6 antagonizes STAT1 function by sequestering nuclear import factors on the rough endoplasmic reticulum/Golgi membrane. J Virol 81:9812–9824. https://doi.org/10.1128/JVI.01012-07.
28. Frieman M, Ratia K, Johnston RE, Mesecar AD, Baric RS. 2009. Severe acute respiratory syndrome coronavirus papain-like protease ubiquitin-like domain and catalytic domain regulate antagonism of IRF3 and NF-κB signaling. J Virol 83:6689–6705. https://doi.org/10.1128/JVI.02220-08.
29. Rabouw HH, Langereis MA, Knaap RCM, Dalebout TJ, Canton J, Sola I, Enjuanes L, Bredenbeek PJ, Kikkert M, de Groot RJ, van Kuppeveld F. 2016. Middle East respiratory coronavirus accessory protein 4a inhibits PKR-mediated antiviral stress responses. PLoS Pathog 12:e1005982-26. https://doi.org/10.1371/journal.ppat.1005982.
30. Menachery VD, Gralinski LE, Mitchell HD, Dinnon KH, Leist SR, Yount BL, Graham RL, McAnarney ET, Stratton KG, Cockrell AS, Debbink K, Sims AC, Waters KM, Baric RS. 2017. Middle East respiratory syndrome coronavirus nonstructural protein 16 is necessary for interferon resistance and viral pathogenesis. mSphere 2:e00346-17. https://doi.org/10.1128/mSphere.00346-17.
31. Deng X, van Geelen A, Buckley AC, O'Brien A, Pillatzki A, Lager KM, Faaberg KS, Baker SC. 2019. Coronavirus endoribonuclease activity in porcine epidemic diarrhea virus suppresses type I and type III interferon responses. J Virol 93:e02000-18. https://doi.org/10.1128/JVI.02000-18.
32. Roth-Cross JK, Bender SJ, Weiss SR. 2008. Murine coronavirus mouse hepatitis virus is recognized by MDA5 and induces type I interferon in brain macrophages/microglia. J Virol 82:9829–9838. https://doi.org/10.1128/JVI.01199-08.
33. Zhou H, Zhao J, Perlman S. 2010. Autocrine interferon priming in macrophages but not dendritic cells results in enhanced cytokine and chemokine production after coronavirus infection. mBio 1:e00219-10. https://doi.org/10.1128/mBio.00219-10.
34. Channappanavar R, Perlman S. 2020. Evaluation of activation and inflammatory activity of myeloid cells during pathogenic human coronavirus infection. Methods Mol Biol 2099:195–204. https://doi.org/10.1007/978-1-0716-0211-9_15.
35. Fung T, Liao Y, Liu D. 2016. Regulation of stress responses and translational control by coronavirus. Viruses 8:184. https://doi.org/10.3390/v8070184.
36. Liu J, HuangFu W-C, Kumar KGS, Qian J, Casey JP, Hamanaka RB, Grigoriadou C, Aldabe R, Diehl JA, Fuchs SY. 2009. Virus-induced unfolded protein response attenuates antiviral defenses via phosphorylation-dependent degradation of the type I interferon receptor. Cell Host Microbe 5:72–83. https://doi.org/10.1016/j.chom.2008.11.008.
37. Laurent-Rolle M, Morrison J, Rajsbaum R, Macleod JML, Pisanelli G, Pham A, Ayllon J, Miorin L, Martinez-Romero C, tenOever BR, García-Sastre A. 2014. The interferon signaling antagonist function of yellow fever virus NS5 protein is activated by type I interferon. Cell Host Microbe 16:314–327. https://doi.org/10.1016/j.chom.2014.07.015.
38. Zhu N, Zhang D, Wang W, Li X, Yang B, Song J, Zhao X, Huang B, Shi W, Lu R, Niu P, Zhan F, Ma X, Wang D, Xu W, Wu G, Gao GF, Tan W. 2020. A novel coronavirus from patients with pneumonia in China, 2019. N Engl J Med 382:727–733. https://doi.org/10.1056/NEJMoa2001017.
39. Huang C, Wang Y, Li X, Ren L, Zhao J, Hu Y, Zhang L, Fan G, Xu J, Gu X, Cheng Z, Yu T, Xia J, Wei Y, Wu W, Xie X, Yin W, Li H, Liu M, Xiao Y, Gao H, Guo L, Xie J, Wang G, Jiang R, Gao Z, Jin Q, Wang J, Cao B. 2020. Clinical features of patients infected with 2019 novel coronavirus in Wuhan, China. Lancet 395:497–506. https://doi.org/10.1016/S0140-6736(20)30183-5.
40. Zhou P, Yang XL, Wang XG, Hu B, Zhang L, Zhang W, Si HR, Zhu Y, Li B, Huang CL, Chen HD, Chen J, Luo Y, Guo H, Jiang RD, Liu MQ, Chen Y, Shen XR, Wang X, Zheng XS, Zhao K, Chen QJ, Deng F, Liu LL, Yan B, Zhan FX, Wang YY, Xiao GF, Shi ZL. 2020. A pneumonia outbreak associated with a new coronavirus of probable bat origin. Nature 579:270–273. https://doi.org/10.1038/s41586-020-2012-7.
41. Afgan E, Baker D, Batut B, van den Beek M, Bouvier D, Čech M, Chilton J, Clements D, Coraor N, Grüning BA, Guerler A, Hillman-Jackson J, Hiltemann S, Jalili V, Rasche H, Soranzo N, Goecks J, Taylor J, Nekrutenko A, Blankenberg D. 2018. The Galaxy platform for accessible, reproducible and collaborative biomedical analyses: 2018 update. Nucleic Acids Res 46:W537–W544. https://doi.org/10.1093/nar/gky379.
42. Kim D, Langmead B, Salzberg SL. 2015. HISAT: a fast spliced aligner with low memory requirements. Nat Methods 12:357–360. https://doi.org/10.1038/nmeth.3317.
43. Liao Y, Smyth GK, Shi W. 2014. featureCounts: an efficient general purpose program for assigning sequence reads to genomic features. Bioinformatics 30:923–930. https://doi.org/10.1093/bioinformatics/btt656.
44. Love MI, Huber W, Anders S. 2014. Moderated estimation of fold change and dispersion for RNA-seq data with DESeq2. Genome Biol 15:550. https://doi.org/10.1186/s13059-014-0550-8.
45. de Hoon MJL, Imoto S, Nolan J, Miyano S. 2004. Open source clustering software. Bioinformatics 20:1453–1454. https://doi.org/10.1093/bioinformatics/bth078.